Geophysical Research Letters

RESEARCH LETTER
10.1029/2021GL093462

Key Points:

- Depth-integrated CbPM-model estimates of net primary production (NPP) from float and satellite data agree within ~40% in the N.E. Pacific
- Depth-resolved CbPM-model estimates of NPP_{float} and NPP_{sat} disagree by >±100%
- NPP was elevated during two recent marine heatwaves, with potential iron fertilization causing anomalously high NPP in 2019

Supporting Information:

Supporting Information may be found in the online version of this article.

Correspondence to:

J. S. Long,
jlong@mbari.org

Citation:

Long, J. S., Fassbender, A. J., & Estapa, M. L. (2021). Depth-resolved net primary production in the Northeast Pacific Ocean: A comparison of satellite and profiling float estimates in the context of two marine heatwaves. *Geophysical Research Letters*, *48*, e2021GL093462. https://doi.org/10.1029/2021GL093462

Received 22 MAR 2021
Accepted 13 SEP 2021

Depth-Resolved Net Primary Production in the Northeast Pacific Ocean: A Comparison of Satellite and Profiling Float Estimates in the Context of Two Marine Heatwaves

J. S. Long[1], A. J. Fassbender[1,2], and M. L. Estapa[3]

[1]Monterey Bay Aquarium Research Institute, Moss Landing, CA, USA, [2]NOAA/OAR Pacific Marine Environmental Laboratory, Seattle, WA, USA, [3]Darling Marine Center, School of Marine Sciences, University of Maine, Walpole, ME, USA

Abstract Methods commonly used to estimate net primary production (NPP) from satellite observations are now being applied to biogeochemical (BGC) profiling float observations. Insights can be gained from regional differences in float and satellite NPP estimates that reveal gaps in our understanding and guide future NPP model development. We use 7 years of BGC profiling float data from the Northeast Pacific Ocean to quantify discrepancies between float and satellite NPP estimates and decompose them into contributions associated with the platform sensing method and depth resolution of observations. We find small, systematic seasonal discrepancies in the depth-integrated NPP (iNPP) but much larger (>±100%) discrepancies in depth-resolved NPP. Annual iNPP estimates from the two platforms are significantly, positively correlated, suggesting that they similarly track interannual variability in the study region. Using the long-term satellite iNPP record, we identify elevated annual iNPP during two recent marine heatwaves and gain insights about ecosystem functionality.

Plain Language Summary Ocean net primary production is equal to gross photosynthesis minus respiration by primary producers, setting the maximum amount of carbon available for export from sunlit surface waters to depths where it can be sequestered from the atmosphere. Quantifying this important piece of the global carbon cycle puzzle is difficult due to the limited number of high-quality, ship-based observations of net primary production. Models have been developed to estimate net primary production from satellite observations; however, heavy cloud cover during winter and sun glint in high-latitude regions remain key challenges. Additionally, satellites observe just the top layer of the sunlit ocean, requiring assumptions to be made when extrapolating through depth. Biogeochemical profiling floats can help to fill remaining observing gaps and improve global net primary production estimates. We use 7 years of float and satellite data from the Northeast Pacific to evaluate how net primary production estimates are impacted by differences in platform detection method and vertical observing resolution. Such comparisons throughout the global ocean will clarify where and how we can leverage the long-term satellite record to study ecosystem events, such as marine heatwaves, and which gaps in our understanding persist.

1. Introduction

Ocean net primary production (NPP) accounts for ~50% of the annual global NPP and sets the baseline for biogenic carbon available to fuel marine ecosystems (Chavez et al., 2011). This metric is used in a variety of ocean biogeochemistry studies, many of which rely on the accuracy of space-born observations. Satellites provide the capability to observe surface ocean ecosystems with near-daily global coverage; however, heavy cloud cover and sun glint in high-latitude regions remain key challenges. Additionally, satellites observe just the top layer of the sunlit ocean, requiring assumptions to be made when extrapolating information through depth. Still, combining satellite products for depth-integrated NPP (Behrenfeld et al., 2005; Behrenfeld & Falkowski, 1997; Westberry et al., 2008) and export efficiency (Dunne et al., 2005; Henson et al., 2011; Laws et al., 2000, 2011) can provide a global estimate of export production—a key metric for setting the atmospheric carbon dioxide concentration (Volk & Hoffert, 1985). While critical to our understanding of the modern global carbon cycle, carbon export estimates derived from remote sensing approaches exhibit a larger meridional gradient than in situ, geochemical estimates (Emerson, 2014; Palevsky et al., 2016; Yang

et al., 2017) and, when integrated globally, span a range of over 100% (5–12 Pg C; Siegel et al., 2016). It remains unclear what fraction of this discrepancy is caused by shortcomings in satellite NPP versus export efficiency estimates due to the paucity of in situ, geochemical observations (e.g., Bisson et al., 2018).

Autonomous platforms equipped with biogeochemical (BGC) sensors can help to fill ecosystem observing gaps by providing year-round, in situ observations throughout the water column and in high-latitude, cloud covered regions. While this observing approach still requires ship-based NPP data for validation, it can supplement the extensive spatiotemporal coverage provided through remote sensing to yield better constrained, and possibly regional, NPP models that are not solely reliant on surface ocean observations as predictor variables. The goal of this work is to evaluate the insights to be gained from quantifying regional differences in satellite and in situ NPP estimates (Friedrichs et al., 2009; Saba et al., 2010, 2011; Sheng et al., 2014) that may reveal gaps in our understanding and lead to improved real-time characterization of ecosystem functionality and variability.

Our study focuses on a relatively homogenous domain, both biogeochemically (Haskell et al., 2020; Plant et al., 2016) and physically (Scannell et al., 2020), of the subarctic northeast Pacific Ocean (48.5°–53°N and 151.5°–139°W; Figure 1a) that has been occupied by BGC profiling floats since 2008. This is a high-nutrient-low-chlorophyll (HNLC) region where iron and light limit primary productivity (Freeland, 2007; Hamme et al., 2010) and nitrate concentrations are normally above detectable limits (Westberry et al., 2016; Whitney & Freeland, 1999; Wong et al., 1999). We use observations from BGC profiling floats to quantify NPP throughout the water column (NPP_{float}) and to derive depth-integrated values ($iNPP_{float}$) for comparison with depth-extrapolated (NPP_{sat}) and depth-integrated ($iNPP_{sat}$) estimates derived from satellite observations, respectively. Our analysis focuses on use of the Carbon-based Productivity Model (CbPM; Behrenfeld et al., 2005; Westberry et al., 2008) and considers how regional carbon cycling assessments could be impacted by the use of satellite-versus float-derived NPP estimates in the absence of NPP validation data.

In the past decade, the NE Pacific has endured two marine heatwaves (MHWs; 2013–2015 and 2018–2020)—more than five consecutive days of sea surface temperature exceeding the 90th percentile of a 30-year historical record (Bond et al., 2015; Hobday et al., 2016; Scannell et al., 2020). A number of studies have evaluated the ecosystem impacts associated with the earlier MHW, including two studies that used BGC-float observations to estimate annual net community production (ANCP; Bif et al., 2019; Yang et al., 2018), which is equal to gross primary production minus community respiration (Laws, 1991). Here, we use a combination of satellite and float-estimated NPP to explore the ecosystem response to anomalous sea surface temperatures.

2. Data

2.1. Float Data

Since 2010, bio-optical measurements have been made by two Teledyne Marine APEX floats (WMO numbers 5903274 and 5903714) and one Sea-Bird Scientific Navis BGCi + pH float (5905988) near OSP where, combined, they have collected near continuous (≤10 day) observations of physical and chemical ocean conditions. Each float carried a conductivity-temperature-depth sensor (SBE 41N, Sea-Bird Scientific), optical nitrate sensor (ISUS, Johnson et al., 2013; or SUNA), bio-optical sensor (APEX: WETLabs ECO FLBB; Navis: MCOMS) measuring chlorophyll fluorescence (470/695 nm) and backscattering (b_{bp}, 700 nm with a scattering angle of 140° for the APEX and 150° for the Navis), and oxygen optode (Aanderaa or SBE63). The Navis float also carried a DeepSea DuraFET pH sensor (Johnson et al., 2016), and its bio-optical sensor also measured colored dissolved organic matter fluorescence (370/460 nm).

Raw and adjusted float data files were downloaded directly from the MBARI FloatViz 6.0 website (http://www.mbari.org/chemsensor/floatviz.htm). The raw files include implementation of the manufacturer calibrations for each sensor while the adjusted files have also undergone more rigorous quality control as outlined in Johnson et al. (2017). Additionally, the shallowest float observation from each profile (~10 m) was extrapolated to the sea surface. This estimation was determined to be adequate based on evaluation of more than 10 years of near-surface variability in fluorescence profiles from Line P cruise observations at OSP. Float profiles were interpolated to 1-m vertical resolution in the upper 200 m. Two floats (5903274 and 5903714) overlapped during 2012, so profiles occurring within 10 day of each other were averaged. The

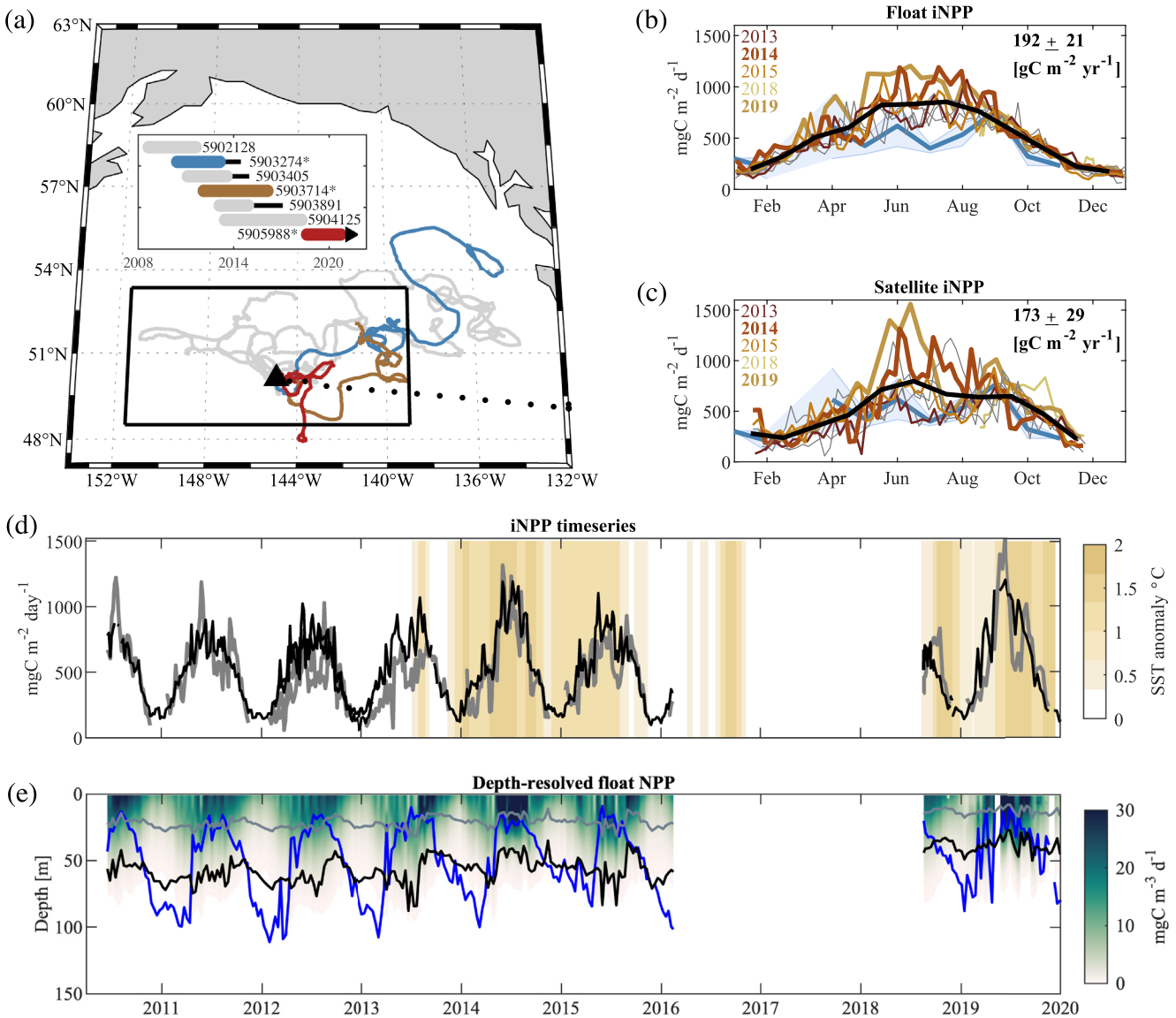

Figure 1. (a) Study region (black rectangle) including Line P cruise stations (black dots), Ocean Station Papa (triangle), and float trajectories. The inset legend lists the float WMO numbers and operational periods. Black lines on the legend correspond to periods when the floats were operating outside of the study region. Asterisks indicate BGC floats with bio-optics used to calculate NPP. Float 5905988 is still operational. Climatologies (black lines) of (b) $iNPP_{float}$ and (c) $iNPP_{sat}$. Inset numbers give the climatological annual iNPP values. iNPP estimates for individual years (gray lines) with MHW years shown in color and heightened iNPP years bolded. A monthly climatology based on shipboard NPP observations from the study region is shown in blue (mean ± 1σ, Table S1). (d) Time series of $iNPP_{sat}$ (gray) and $iNPP_{float}$ (black) with positive sea surface temperature anomalies shown in the background (tan). (e) Depth-resolved NPP_{float} time series including float estimates of mixed layer depth (blue), first optical depth (gray), and euphotic zone depth (black).

original, unaveraged data are used in Figures 1b and 1d. The averaged data from these two floats are used in subsequent figures and tables.

2.2. Satellite, Model, and Hydrographic Data

Ocean color products derived from the Moderate Resolution Imaging Spectroradiometer (MODIS) aboard the NASA Aqua satellite used for this analysis include 0.17° resolution, 8-day averaged chlorophyll-*a* concentrations (Chl; Garver-Siegel-Maritorena algorithm, Morel & Maritorena, 2001), particulate backscatter (b_{bp}), CbPM-NPP (Westberry et al., 2008), and Photosynthetically Available Radiation (PAR). These data and monthly estimates of mixed layer depth from the Hybrid-Coordinate Ocean Model (HYCOM) were

downloaded from the mission start date (July 2002) to January 2020 from the Oregon State Ocean Productivity Group website (http://sites.science.oregonstate.edu/ocean.productivity/custom.php; Figure S1). Monthly nitrate climatology data from the World Ocean Atlas (WOA; https://www.ncei.noaa.gov/access/world-ocean-atlas-2018/) were used to estimate the nitracline depth for satellite-based CbPM calculations. The satellite CbPM-NPP estimates are reported herein as values extracted nearest in time and location to float sampling (NPP_{sat}, Figure S1) or averaged over the study region ($NPP_{sat\text{-}xy}$; black box, Figure 1a). Geochemical estimates of iNPP using clean techniques for ^{13}C or ^{14}C 24-hr incubations (Table S1) from previously reported data sets (Booth et al., 1988; Boyd & Harrison, 1999; Giesbrecht, 2010; Kawakami et al., 2010; Miller et al., 1991; Timmerman & Hamme, 2021; Welschmeyer et al., 1993; Wong et al., 1995) are compared with the seasonal cycles of $iNPP_{float}$ and $iNPP_{sat}$.

Monthly sea surface temperature (SST) anomalies were calculated using the MATLAB package described in Jacox et al. (2020). SST anomalies (Figure 1d) were identified using the daily, NOAA Optimum Interpolation SST product (version 2; https://psl.noaa.gov/data/gridded/data.noaa.oisst.v2.html) at 0.25° resolution (Banzon et al., 2016; Reynolds et al., 2007). Annual SST anomalies were computed using the full SST data record (1982–2019) averaged over the study region (SST_{xy}). To achieve the best float-chlorophyll estimate possible, we relied on discrete fluorometric measurements of extracted Chl (mg m^{-3}), adjusted to HPLC data provided by Dr. Angelica Peña (IOS, https://open.canada.ca/data/en/dataset/871b0b32-3135-40c8-868e-c5d87800ca76), collected during the Canadian Line P cruises (Figure S3; http://www.waterproperties.ca/linep/cruises.php).

3. Methods

3.1. Fluorescence-to-Chlorophyll Concentration Conversion

Float fluorometers were calibrated using laboratory standards prior to deployment. Similar to previous analyses (Roesler et al., 2017), we found the laboratory calibrations to be inadequate for determining Chl over the full float lifetime, especially for the MCOMS sensor (WMO 5905988; Figure S2). Possible explanations include changes in phytoplankton community composition; photoadaptive responses of phytoplankton in iron-limited regions that cause the fluorescence-to-Chl relationship to change over time (Behrenfeld & Milligan, 2013); or other fitness factors. Raw float fluorescence data were corrected for nonphotochemical quenching (Xing et al., 2012) before a background signal (minimum Chl between 100 and 300 m) was subtracted from each profile (Broenkow et al., 1983; Xing et al., 2017). Annual relationships between fluorescence and Chl were defined using ship-based Line P observations (Figures S4 and S5) and were subsequently used to adjust the float fluorescence data (see Text S1 for details).

3.2. Backscatter to Phytoplankton Carbon Conversion

Particulate backscatter was estimated following Johnson et al. (2017), and signals due to large particles, zooplankton, refractory backscattering, and instrument noise were removed (Briggs et al., 2020; see Text S2 for details). Estimates of phytoplankton carbon concentrations (C; mg m^{-3}) were calculated using the relationship of Behrenfeld et al. (2005) by first converting b_{bp} at 700 nm to b_{bp} at 443 nm assuming a power law dependence on wavelength with a power law slope parameter set to −1 (Morel & Maritorena, 2001):

$$C = 13{,}000 \times \left(b_{bp}(443) - 0.00035\right). \quad (1)$$

3.3. Float-Based Net Primary Production

In CbPM, NPP is the product of C and growth rate, both of which can be estimated from float or satellite observations. CbPM-NPP is calculated using mixed layer depth, Chl, b_{bp}, PAR, the diffuse attenuation coefficient at 490 nm (K_d[490]), and an estimate of the nitracline depth. Float-estimated mixed layer depths were calculated using the density algorithm of Holte and Talley (2009). K_d(490) and K_d(PAR) were estimated using float Chl and the relationship described in Morel et al. (2007) (their Equations 8 and 9, respectively). Following the approach of previous studies to adapt CbPM for profiling float applications (Estapa et al., 2019; Yang et al., 2021), satellite PAR was attenuated with depth using the depth-resolved estimates of

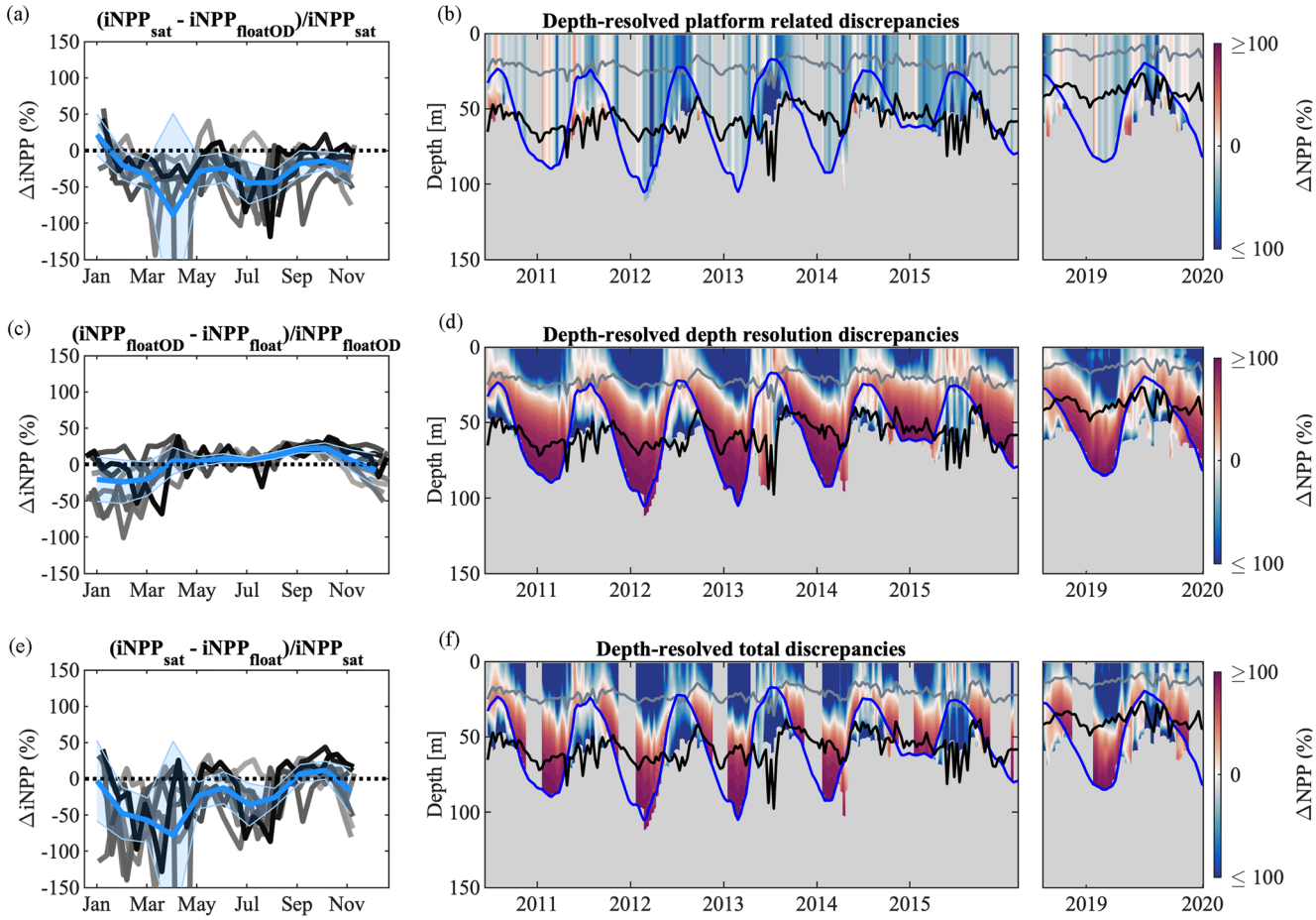

Figure 2. Annual (greys) and climatological (light blue; mean ± 1σ) discrepancies between CbPM calculation methods (values given in Table S2). Relative differences between (a) iNPP$_{sat}$ and iNPP$_{floatOD}$, (c) iNPP$_{floatOD}$, and iNPP$_{float}$, (e) iNPP$_{sat}$ and iNPP$_{float}$. (b, d, and f) Depth-resolved relative discrepancies in NPP including HYCOM mixed layer depths (blue) and float estimates of z_{OD} (gray) and z_{eu} (black). Relative differences between NPP$_{floatOD}$ and NPP$_{float}$ above z_{OD} occur when there are multiple float observations recorded within this depth range. NPP values < 0.5 mg C m^{-3} d^{-1} were set to NaN. Consistent wintertime breaks in section plots (b) and (f) reflect observing gaps in the satellite data. Absolute discrepancy values are shown in Figure S6.

K_d(PAR). The euphotic zone depth (z_{eu}) was calculated as 4.6/K_d (PAR), and the first optical depth (z_{OD}) was calculated as 1/K_d(PAR). NPP$_{float}$ and NPP$_{sat}$ values were integrated from the surface to 200 m, well below the deepest winter mixing depth.

4. Results

4.1. Float Versus Satellite CbPM-NPP

Satellite and float CbPM-estimates of iNPP agree relatively well when integrated through 200 m (Figure 1d): the mean absolute relative difference, with respect to iNPP$_{sat}$, is 35%. Over 90% of the discrete NPP observations from our study region were made prior to 1990 (Table S1), such that direct validation of the float or satellite estimates is not feasible. As expected, discrepancies were found between the discrete climatology and both the iNPP$_{sat}$ and iNPP$_{float}$ climatologies (Figures 1b and 1c). The largest discrepancies between iNPP$_{sat}$ and iNPP$_{float}$ climatologies occur in late winter and early spring (Figure 2e and Table S2) when differences range from −23% to −78%, relative to iNPP$_{sat}$.

To understand what is causing the observed discrepancies, we consider two important methodological differences between the iNPP$_{float}$ and iNPP$_{sat}$ calculations. The first difference is associated with using remote (satellite) versus in situ (float) observations of Chl and b_{bp} (platform related discrepancies; Bisson et al., 2020). The second difference is associated with the extrapolation of satellite observations to depth

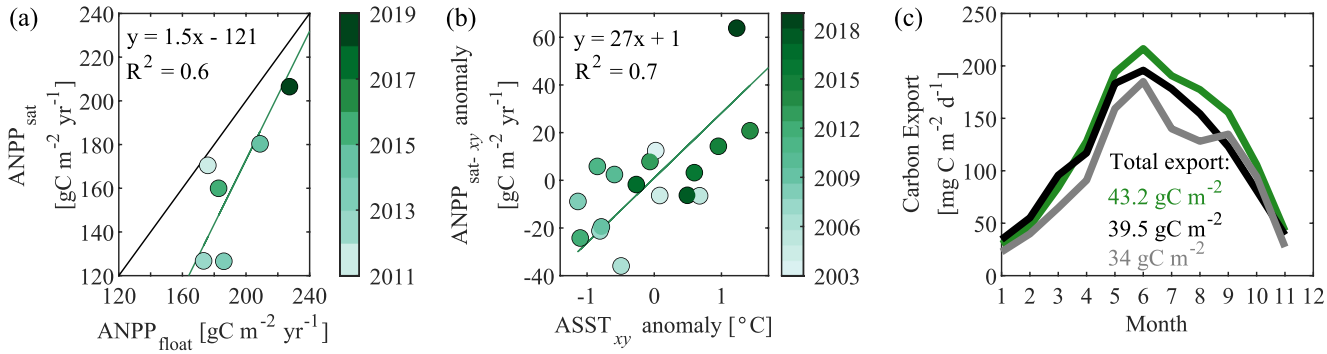

Figure 3. (a) $ANPP_{float}$ versus $ANPP_{sat}$. Black line is 1:1. (b) Annual SST ($ASST_{xy}$) anomaly versus $ANPP_{sat\text{-}xy}$. (c) Climatologies of export calculated as the product of satellite-estimated e-ratio (Laws et al., 2011, Equation 3) and $iNPP_{floatOD}$ (green), $iNPP_{float}$ (black), or $iNPP_{sat}$ (gray).

versus using depth-resolved float observations (depth-resolution discrepancies; Saba et al., 2010). Specifically, the satellite CbPM approach assumes a homogeneous mixed layer followed by an exponential decay of growth rate with depth.

To isolate the first methodological difference, float Chl and b_{bp} values were averaged within z_{OD} to serve as a proxy for what the satellite observes. Then, NPP was derived through depth using the same method of CbPM applied to satellite data (Westberry et al., 2008), including satellite estimates of mixed layer depth, PAR, and nitracline, with float z_{OD}-averaged data of Chl and b_{bp}. Discrepancies between the resulting float ($iNPP_{floatOD}$) and $iNPP_{sat}$ values therefore reflect differences in Chl and b_{bp} observations. The $iNPP_{sat}$ and $iNPP_{floatOD}$ climatologies reveal a seasonally varying bias, with the largest relative differences (~50%) during spring and summer and the smallest relative differences (~1%) during winter (Figure 2a and Table S2). The differences are constant throughout the mixed layer where the CbPM algorithm assumes a fixed Chl:C (Figure 2b).

To isolate the second methodological difference, we compare $NPP_{floatOD}$ and NPP_{float}. The seasonal bias in iNPP resulting from the CbPM-model assumptions required to extend surface observations with depth is smaller in magnitude than the bias associated with observing platform differences. However, this is largely due to the compensation of biases when integrated through depth (Figure 2c). There is a slight overestimation (1–30%) of $NPP_{floatOD}$ throughout the mixed layer during summer and significant overestimation and underestimation (exceeding ±100%) of $NPP_{floatOD}$ at different depths within the mixed layer (spanning a range of NPP values, up to 20 mg C m^{-3} d^{-1}; see Figure 1e) during fall, winter, and spring. Therefore, biases resulting from the depth-resolution discrepancy are more important when considering depth-resolved, rather than depth-integrated, NPP in this region.

The combined effect of the two methodological differences in $iNPP_{float}$ and $iNPP_{sat}$ calculations near OSP is a seasonally consistent, partially compensating bias (Figures 2e, 2f and S7). Both the platform and depth-resolution discrepancies contribute to the lower spring $iNPP_{sat}$ values (−53%) while the platform discrepancies largely explain the lower $iNPP_{sat}$ values during ~July, which leads to the double hump in production (Figure 1c) that is not found in the $iNPP_{float}$ climatology. The main differences in iNPP are dominated by observing platform differences. However, the depth-resolved NPP values differ by significantly larger margins (up to ±900%), emphasizing that depth-extrapolation may be a significant source of uncertainty in evaluations of vertically resolved NPP_{sat}.

4.2. Annual iNPP

Annual iNPP (ANPP) values were calculated from January through December for each year (Figure 3a and Table S3). $ANPP_{float}$ was not calculated if floats were missing observations from more than one month and satellite ANPP was calculated (a) from data extracted nearest in time and space to each float ($ANPP_{sat}$; Figure 1a) and (b) as a spatial average ($ANPP_{sat\text{-}xy}$) over the study region (Figure 1b). Missing NPP_{sat} values, caused by cloud cover in December, were filled via interpolation. The highest $ANPP_{float}$, $ANPP_{sat}$, and $ANPP_{sat\text{-}xy}$ values were found during MWHs in 2014 and 2019. Though there exist moderate, systematic

seasonal differences between $iNPP_{float}$ and $iNPP_{sat}$ (Figure 2e), a significant, positive relationship between float and satellite ANPP values (Figure 3a) suggests that both platforms provide a consistent perspective on interannual variability. As such, we leverage the time periods of both platforms to analyze ANPP anomalies with respect to annual SST anomalies.

5. Marine Heatwaves and NPP

Two marine heatwaves occurred in the NE Pacific during the study period: the first from 2013 to 2016 followed by one from mid-2018 to 2020. Previous studies on the ecosystem impacts associated with the 2013–2016 MHW in the NE Pacific and nearby regions have focused on changes in species biomass, biogeographical shifts, and large-scale die-offs and mass strandings of marine mammals, fish, and birds (Brodeur et al., 2019; Cavole et al., 2016; Cheung & Frölicher, 2020; Yang et al., 2019). Others have evaluated changes in phytoplankton community composition (Peña et al., 2019), habitat threats and redistribution (Jacox et al., 2020; Smale et al., 2019), harmful algal blooms (McCabe et al., 2016; Trainer et al., 2020), and changes in annual net community production (ANCP; Bif et al., 2019; Yang et al., 2018). To our knowledge, no studies have focused on how MHWs influence NPP in this region.

$ANPP_{sat\text{-}xy}$ anomalies are positively correlated with $ASST_{xy}$ anomalies (Figure 3b), suggesting that up to 70% of the ANPP variability in the region may be related to environmental changes associated with elevated water temperatures. The 2018–2020 MWH was like the 2013–2016 MHW in that the upper ocean exhibited intensified stratification and winter mixing did not persistently penetrate the 25.5 kg m^{-3} potential density surface (Figure S8). However, the earlier MHW exhibited a larger, positive thermal anomaly and the later MHW exhibited a larger, negative salinity anomaly in the upper ocean (Scannell et al., 2020). Elevated NPP, in both float and satellite records, was found during summer following the first winter of each MHW (2014/2019); preceded by early heightened growth rates (Figure S9). Prior studies of the 2013–2016 MHW identified increases in phytoplankton accumulation and Chl during summer of 2014 (Cavole et al., 2016; Peña et al., 2019). In 2019, we also find elevated surface Chl and phytoplankton carbon values and depressed carbon dioxide partial pressures, estimated from float pH observations (Johnson et al., 2017; Williams et al., 2016; Figures S2b and S8). Further, phytoplankton growth rates have been shown to be temperature dependent (Barton & Yvon-durocher, 2019; Laws et al., 2000). Though ANPP values were high during both MHWs, only the 2019 ANPP values were statistically significant in both the satellite and float records (Table S3).

Elevated ANPP during MHWs may seem unintuitive because stratification also limits the entrainment of denser, nutrient-rich waters; however, the study domain is an HNLC region where productivity is primarily limited by light and iron availability (Maldonado et al., 1999). Shortwave radiation data from the OSP mooring suggest that light availability was not anomalous during 2014 or 2019. Possible sources of iron supply to the region include intermediate water transport and advection (Harrison et al., 1999; Nishioka et al., 2020), fire ash deposition (Abram et al., 2003; Kramer, 2020), Asian and Alaskan dust (Boyd et al., 1998), and volcanic ash (Hamme et al., 2010; Westberry et al., 2019). Notably, the June 22, 2019 Raikoke volcanic eruption resulted in exceptionally high sulfur dioxide concentrations (Figure S10; Theys et al., 2019) over the study region in July based on the Ozone Monitoring Instrument aboard the Aura satellite. Additionally, anomalously high Aerosol Optical Depths (an indicator of smoke from wildfires, dust, and sulfates) over Alaska and Canada were observed in MODIS-Terra satellite imagery from May through July of 2019 (Figure S10), overlapping an unprecedented fire season in Southcentral Alaska (Bhatt et al., 2021). Thus, it is possible that iron supply from volcanic ash and regional fires may have caused the anomalous 2019 primary productivity. Another key factor suggesting elevated production during 2019 is that mixed layer nitrate concentrations were depleted to the float sensor detection limit in August (Figure S8); something not seen in at least 13 years of seasonal Line P observations and 8 years of continuous float observations near OSP.

Float-based estimates of ANCP during the 2013–2016 MHW by Yang et al. (2018) and Bif et al. (2019), who used different chemical tracers, suggest reduced ANCP in different years of the warm event. Lower-than-average ANCP coupled with higher-than-average ANPP suggests that interannual variability in heterotrophic respiration may play an important role in regulating upper ocean carbon cycling and the efficiency of carbon export. Since NPP appears to have been elevated during both recent MHWs, the negative impacts

experienced by higher trophic levels during the earlier MHW suggest that the base of the food chain may not be a good indicator for broader ecosystem responses.

6. Conclusions

Over 80% of the global surface ocean has begun to show increases in the duration and intensity of MHWs, including the NE Pacific (Oliver et al., 2018), which are expected to become more frequent under global warming (Frölicher et al., 2018). Our ANPP estimates are positively correlated with annual SST anomalies; however, exceptionally anomalous conditions during 2019, including a volcanic eruption and unprecedented regional fire activity, make it difficult to draw firm conclusions about the general ecosystem response to MHWs.

As NPP models become more commonly applied to float observations, our work suggests that consideration of both depth-integrated and depth-extrapolated biases is needed, in addition to platform observing differences. We find a persistent seasonal discrepancy between depth-integrated NPP (iNPP) estimates from depth-resolved float data and depth-extrapolated satellite data throughout the study region. Satellite iNPP estimates appear to miss the late winter and early spring bloom initiation relative to float iNPP estimates that capture subsurface variability and are not limited by cloud cover. While iNPP estimates from these platforms are similar (within ∼50%) and covary, depth-resolved NPP discrepancies are large (≥±100%) and can reach up to ±900%. Though we are limited by a lack of discrete NPP data in our ability to ascertain which of the platforms provides a more accurate estimate of NPP, we might expect the float estimates to better reflect subsurface variability within the mixed layer (Carranza et al., 2018). Additionally, the rigorous QC applied to the float fluorescence data elevates our confidence in these estimates. The preadjusted float fluorescence data would have yielded a poor estimate of Chl, leading to large, unconstrained biases in calculated NPP (Figure S11). Additionally, due to the nonlinear Chl:fluorescence relationship with depth (Figure S2), satellite observations of Chl are not sufficient to adjust subsurface float fluorescence data; significant biases remain in float Chl profiles corrected using satellite surface observations.

Seasonally persistent discrepancies between depth-resolved and depth-extrapolated iNPP estimates have important implications for regional, and potentially global, carbon cycle studies that use profiling float and satellite observing approaches interchangeably. For example, the same e-ratio (Laws et al., 2011, Equation 3) applied to float and satellite iNPP climatologies from our study region yields export estimates that differ by 12% when integrated annually (Figure 3c). Larger differences may be expected in less physically quiescent ocean regions where annual mixed layer depths are more variable and the vertical resolution of observations may be more important. Discrete NPP validation data are needed to assess the accuracy of CbPM (and other NPP algorithms) in more regions and to develop new algorithms that can leverage the growing BGC-float array to fill gaps in, and add context to, surface satellite observations. In the meantime, characterizing iNPP biases caused by observing platform and depth-resolution differences between float and satellite approaches in other ocean regions would be useful. Such efforts, in combination with similar work to compare and improve satellite e-ratio algorithms (e.g., Haskell et al., 2020), may help to reduce the >100% spread in annual global carbon export estimates.

Data Availability Statement

Raw and adjusted float data files were downloaded directly from the MBARI FloatViz 6.0 website (http://www.mbari.org/chemsensor/floatviz.htm). Input data for CbPM-NPP included HYCOM-MLD and satellite ocean color data (PAR, Chl, and b_{bp}) provided by the Oregon State Ocean Productivity Group (http://sites.science.oregonstate.edu/ocean.productivity/custom.php), and monthly nitrate climatology data (WOA; https://www.ncei.noaa.gov/access/world-ocean-atlas-2018/). Other data used in this study include, monthly SST data (NOAA OISSTv2; https://psl.noaa.gov/data/gridded/data.noaa.oisst.v2.html), HPLC data (IOS, https://open.canada.ca/data/en/dataset/871b0b32-3135-40c8-868e-c5d87800ca76; record ID: 871b0b32-3135-40c8-868e-c5d87800ca76), Canadian Line P cruise data (http://www.waterproperties.ca/linep/cruises.php), Station Papa mooring data (https://www.ncei.noaa.gov/data/oceans/ncei/ocads/data/0100074/), SO_2 Column Amount and AOD (OMI OMSO2e v003 and MODIS-Terra MOD08_M3 v6.1; https://giovanni.gsfc.nasa.gov/).

Acknowledgments
The authors are grateful to the MBARI Chemical Sensor Lab for their maintenance of quality-controlled, BGC-float data, the OSU Biological Productivity group for providing processed satellite and mixed layer depth data used in the calculation of satellite-based NPP, the captain and crew of the CCGS John P. Tully, and the Institute of Ocean Sciences at the Department of Fisheries and Oceans Canada for years of data provided through the Line P Program. The authors thank Joshua Plant for sharing his knowledge in BGC-float sensors and Mariana Bif for assistance with b_{bp} data quality control, the captain and crew of the R. V. Sally Ride as well as Scott Freeman and Mary Jane Perry for a recent float deployment during the North Pacific EXPORTS occupation. The authors thank the UW Riser Lab for assistance with float deployment logistics and quality control of physical sensor data. The authors thank the two anonymous reviewers for their valuable suggestions throughout the review process. All data used in this analysis are publicly available and can be accessed using the links provided in the data section of the manuscript. This work was made possible by support from the David and Lucile Packard Foundation and the National Science Foundation (A. Fassbender; OCE1756932). This is PMEL Contribution No. 5203.

References

Abram, N. J., Gagan, M. K., McCulloch, M. T., Chappell, J., & Hantoror, W. S. (2003). Coral reef death during the 1997 Indian Ocean dipole linked to Indonesian wildfires. *Science*, *301*(5635), 952–955. https://doi.org/10.1126/science.1083841

Banzon, V., Smith, T. M., Liu, C., & Hankins, W. (2016). A long-term record of blended satellite and in situ sea surface temperature for climate monitoring, modeling and environmental studies. *Earth System Science Data Discussions*, *8*, 165–176. https://doi.org/10.5194/essd-2015-44

Barton, S., & Yvon-durocher, G. (2019). Quantifying the temperature dependence of growth rate in marine phytoplankton within and across species. *Limnology & Oceanography*, *64*, 2081–2091. https://doi.org/10.1002/lno.11170

Behrenfeld, M. J., Boss, E., Siegel, D. A., Shea, D. M., Behrenfeld, M. J., Boss, E., et al. (2005). Carbon-based ocean productivity and phytoplankton physiology from space. *Global Biogeochemical Cycles*, *19*, GB1006. https://doi.org/10.1029/2004GB002299

Behrenfeld, M. J., & Falkowski, P. G. (1997). Photosynthetic rates derived from satellite-based chlorophyll concentration. *Limnology & Oceanography*, *42*(1), 1–20. https://doi.org/10.4319/lo.1997.42.1.0001

Behrenfeld, M. J., & Milligan, A. J. (2013). Photophysiological expressions of iron stress in phytoplankton. *Annual Review of Marine Science*, *5*(1), 217–246. https://doi.org/10.1146/annurev-marine-121211-172356

Bhatt, U. S., Lader, R. T., Walsh, J. E., Bieniek, P. A., Thoman, R., Berman, M., et al. (2021). Emerging anthropogenic influences on the Southcentral Alaska temperature and precipitation extremes and related fires in 2019. *Land*, *10*(1), 82.

Bif, M. B., Siqueira, L., & Hansell, D. A. (2019). Warm events induce loss of resilience in organic carbon production in the Northeast Pacific Ocean. *Global Biogeochemical Cycles*, *33*, 1174–1186. https://doi.org/10.1029/2019GB006327

Bisson, K. M., Boss, E. S., Werdell, P. J., Ibrahim, A., & Behrenfeld, M. J. (2020). Particulate backscattering in the Global Ocean: A comparison of independent assessments. *Geophysical Research Letters*, *48*, e2020GL090909. https://doi.org/10.1029/2020GL090909

Bisson, K. M., Siegel, D. A., DeVries, T., Cael, B. B., & Buesseler, K. O. (2018). How data set characteristics influence ocean carbon export models. *Global Biogeochemical Cycles*, *32*, 1312–1328. https://doi.org/10.1029/2018GB005934

Bond, N. A., Cronin, M. F., Freeland, H., & Mantua, N. (2015). Causes and impacts of the 2014 warm anomaly in the NE Pacific. *Geophysical Research Letters*, *42*, 3414–3420. https://doi.org/10.1002/2015GL063306

Booth, B. C., Lewin, J., & Lorenzen, C. J. (1988). Spring and summer growth rates of subarctic Pacific phytoplankton assemblages determined from carbon uptake and cell volumes estimated using epifluorescence microscopy. *Marine Biology*, *98*(2), 287–298. https://doi.org/10.1007/BF00391207

Boyd, P., & Harrison, P. J. (1999). Phytoplankton dynamics in the NE subarctic Pacific. *Deep-Sea Research Part II Topical Studies in Oceanography*, *46*(11–12), 2405–2432. https://doi.org/10.1016/S0967-0645(99)00069-7

Boyd, P. W., Wong, C. S., Merrill, J., Whitney, F., Snow, J., Harrison, P. J., & Al, B. E. T. (1998). Atmospheric iron supply and enhanced vertical carbon flux in the NE subarctic Pacific: Is there a connection? *Global Biogeochemical Cycles*, *12*(3), 429–441. https://doi.org/10.1029/98GB00745

Briggs, N., Dall'Olmo, G., & Claustre, H. (2020). Major role of particle fragmentation in regulating biological sequestration of CO_2 by the oceans. *Science*, *367*(6479), 791–793. https://doi.org/10.1126/science.aay1790

Brodeur, R. D., Auth, T. D., & Phillips, A. J. (2019). Major shifts in pelagic micronekton and macrozooplankton community structure in an upwelling ecosystem related to an unprecedented marine heatwave. *Frontiers in Marine Science*, *6*, 1–15. https://doi.org/10.3389/fmars.2019.00212

Broenkow, W. W., Lewitus, A. J., Yarbrough, M. A., & Krenz, R. T. (1983). Particle fluorescence and bioluminescence distributions in the eastern tropical Pacific. *Nature*, *302*, 329–331. https://doi.org/10.1038/302329a0

Carranza, M. M., Gille, S. T., Franks, P. J. S., Johnson, K. S., Pinkel, R., & Girton, J. B. (2018). When mixed layers are not mixed. Storm-driven mixing and bio-optical vertical gradients in mixed layers of the Southern Ocean. *Journal of Geophysical Research: Oceans*, *123*, 7264–7289. https://doi.org/10.1029/2018JC014416

Cavole, L. M., Demko, A. M., Diner, R. E., Giddings, A., Koester, I., Pagniello, C. M. L. S., et al. (2016). Biological impacts of the 2013–2015 warm-water anomaly in the northeast Pacific: Winners, Losers, and the Future. *Oceanography*, *29*(2), 273–285. https://doi.org/10.5670/oceanog.2016.32

Chavez, F. P., Messié, M., & Pennington, J. T. (2011). Marine primary production in relation to climate variability and change. *Annual Review of Marine Science*, *3*, 227–260. https://doi.org/10.1146/annurev.marine.010908.163917

Cheung, W. W. L., & Frölicher, T. L. (2020). Marine heatwaves exacerbate climate change impacts for fisheries in the northeast Pacific. *Scientific Reports*, *10*(1), 1–10. https://doi.org/10.1038/s41598-020-63650-z

Dunne, J. P., Armstrong, R. A., Gnnadesikan, A., & Sarmiento, J. L. (2005). Empirical and mechanistic models for the particle export ratio. *Global Biogeochemical Cycles*, *19*, GB4026. https://doi.org/10.1029/2004GB002390

Emerson, S. (2014). Annual net community production and the biological carbon flux in the ocean. *Global Biogeochemical Cycles*, *28*, 14–28. https://doi.org/10.1002/2013GB004680

Estapa, M. L., Feen, M. L., & Breves, E. (2019). Direct observations of biological carbon export from profiling floats in the Subtropical North Atlantic. *Global Biogeochemical Cycles*, *33*, 282–300. https://doi.org/10.1029/2018GB006098

Freeland, H. (2007). A short history of Ocean Station Papa and Line P. *Progress in Oceanography*, *75*(2), 120–125. https://doi.org/10.1016/j.pocean.2007.08.005

Friedrichs, M. A. M., Carr, M. E., Barber, R. T., Scardi, M., Antoine, D., Armstrong, R. A., et al. (2009). Assessing the uncertainties of model estimates of primary productivity in the tropical Pacific Ocean. *Journal of Marine Systems*, *76*(1–2), 113–133. https://doi.org/10.1016/j.jmarsys.2008.05.010

Frölicher, T. L., Fischer, E. M., & Gruber, N. (2018). Marine heatwaves under global warming. *Nature*, *560*(7718), 360–364. https://doi.org/10.1038/s41586-018-0383-9

Giesbrecht, K. (2010). *Biological productivity in the Northeast Pacific: Comparing an in-situ method with incubation based methods*. University of Victoria.

Hamme, R. C., Webley, P. W., Crawford, W. R., Whitney, F. A., Degrandpre, M. D., Emerson, S. R., et al. (2010). Volcanic ash fuels anomalous plankton bloom in subarctic northeast Pacific. *Geophysical Research Letters*, *37*, L19604. https://doi.org/10.1029/2010GL044629

Harrison, P. J., Boyda, P. W., Varela, D. E., Takeda, S., Shiomoto, A., & Odate, T. (1999). Comparison of factors controlling phytoplankton productivity in the NE and NW subarctic Pacific gyres. *Progress in Oceanography*, *43*(2–4), 205–234. https://doi.org/10.1016/S0079-6611(99)00015-4

Haskell, W. Z., Fassbender, A. J., Long, J. S., & Plant, J. N. (2020). Annual net community production of particulate and dissolved organic carbon from a decade of biogeochemical profiling float observations in the Northeast Pacific. *Global Biogeochemical Cycles*, *34*, e2020GB006599. https://doi.org/10.1029/2020GB006599

Henson, S. A., Sanders, R., Madsen, E., Morris, P. J., Le Moigne, F., & Quartly, G. D. (2011). A reduced estimate of the strength of the ocean's biological carbon pump. *Geophysical Research Letters*, *38*, L04606. https://doi.org/10.1029/2011GL046735

Hobday, A. J., Alexander, L. V., Perkins, S. E., Smale, D. A., Straub, S. C., Oliver, E. C. J., et al. (2016). A hierarchical approach to defining marine heatwaves. *Progress in Oceanography*, *141*, 227–238. https://doi.org/10.1016/j.pocean.2015.12.014

Holte, J., & Talley, L. (2009). A new algorithm for finding mixed layer depths with applications to argo data and subantarctic mode water formation. *Journal of Atmospheric and Oceanic Technology*, *26*(9), 1920–1939. https://doi.org/10.1175/2009JTECHO543.1

Jacox, M. G., Alexander, M. A., Bograd, S. J., & Scott, J. D. (2020). Thermal displacement by marine heatwaves. *Nature*, *584*(7819), 82–86. https://doi.org/10.1038/s41586-020-2534-z

Johnson, K. S., Coletti, L. J., Jannasch, H. W., Sakamoto, C. M., Swift, D. D., & Riser, S. C. (2013). Long-term nitrate measurements in the ocean using the in situ ultraviolet spectrophotometer: Sensor integration into the APEX profiling float. *Journal of Atmospheric and Oceanic Technology*, *30*(8), 1854–1866. https://doi.org/10.1175/JTECH-D-12-00221.1

Johnson, K. S., Jannasch, H. W., Coletti, L. J., Elrod, V. A., Martz, T. R., Takeshita, Y., et al. (2016). Deep-sea DuraFET: A pressure tolerant pH sensor designed for global sensor networks. *Analytical Chemistry*, *88*(6), 3249–3256. https://doi.org/10.1021/acs.analchem.5b04653

Johnson, K. S., Plant, J. N., Coletti, L. J., Jannasch, H. W., Sakamoto, C. M., Riser, S. C., et al. (2017). Biogeochemical sensor performance in the SOCCOM profiling float array. *Journal of Geophysical Research: Oceans*, *122*, 6416–6436. https://doi.org/10.1002/2017JC012838

Kawakami, H., Honda, M. C., Matsumoto, K., Fujiki, T., & Watanabe, S. (2010). East-west distribution of POC fluxes estimated from 234 Th in the Northern North Pacific in Autumn. *Journal of Oceanography*, *66*, 71–83. https://doi.org/10.1007/s10872-010-0006-z

Kramer, S. J., Bisson, K. M., & Fischer, A. D. (2020). Observations of phytoplankton community composition in the Santa Barbara channel during the Thomas Fire. *Journal of Geophysical Research: Oceans*, *125*, e2020JC016851. https://doi.org/10.1029/2020JC016851

Laws, E. A. (1991). Photosynthetic quotients, new production and net community production in the open ocean. *Deep Sea Research Part A*, *38*, 143–167. https://doi.org/10.1016/0198-0149(91)90059-O

Laws, E. A., D'Sa, E., & Naik, P. (2011). Simple equations to estimate ratios of new or export production to total production from satellite-derived estimates of sea surface temperature and primary production. *Limnology and Oceanography: Methods*, *9*, 593–601. https://doi.org/10.4319/lom.2011.9.593

Laws, E. A., Falkowski, P. G., Smith, W. O., Ducklow, H., & McCarthy, J. J. (2000). Temperature effects on export production in the open ocean. *Global Biogeochemical Cycles*, *14*(4), 1231–1246. https://doi.org/10.1029/1999GB001229

Maldonado, M. T., Boyd, P. W., Harrison, P. J., & Price, N. M. (1999). Co-limitation of phytoplankton growth by light and Fe during winter in the NE subarctic Pacific Ocean. *Deep-Sea Research Part II: Topical Studies in Oceanography*, *46*, 2475–2485. https://doi.org/10.1016/s0967-0645(99)00072-7

McCabe, R. M., Hickey, B. M., Kudela, R. M., Lefebvre, K. A., Adams, N. G., Bill, B. D., et al. (2016). An unprecedented coastwide toxic algal bloom linked to anomalous ocean conditions. *Geophysical Research Letters*, *43*, 10366–10376. https://doi.org/10.1002/2016GL070023

Miller, C. B., Frost, B. W., Wheeler, P. A., Land-y, M. R., Welschmeyer, N., & Powell, T. M. (1991). Ecological dynamics in the subarctic Pacific, a possibly iron-limited ecosystem. *Limnology & Oceanography*, *36*(8), 1600–1615. https://doi.org/10.4319/lo.1991.36.8.1600

Morel, A., Huot, Y., Gentili, B., Werdell, P. J., Hooker, S. B., & Franz, B. A. (2007). Examining the consistency of products derived from various ocean color sensors in open ocean (Case 1) waters in the perspective of a multi-sensor approach. *Remote Sensing of Environment*, *111*(1), 69–88. https://doi.org/10.1016/j.rse.2007.03.012

Morel, A., & Maritorena, S. (2001). Bio-optical properties of oceanic waters: A reappraisal. *Journal of Geophysical Research*, *106*(C4), 7163–7180. https://doi.org/10.1029/2000JC000319

Nishioka, J., Obata, H., Ogawa, H., Ono, K., Yamashita, Y., Lee, K., et al. (2020). Subpolar marginal seas fuel the North Pacific through the intermediate water at the termination of the global ocean circulation. *Proceedings of the National Academy of Sciences of the United States of America*, *117*(23), 12665–12673. https://doi.org/10.1073/pnas.2000658117

Oliver, E. C. J., Donat, M. G., Burrows, M. T., Moore, P. J., Smale, D. A., Alexander, L. V., et al. (2018). Longer and more frequent marine heatwaves over the past century. *Nature Communications*, *9*(1), 1–12. https://doi.org/10.1038/s41467-018-03732-9

Palevsky, H. I., Quay, P. D., & Nicholson, D. P. (2016). Discrepant estimates of primary and export production from satellite algorithms, a biogeochemical model, and geochemical tracer measurements in the North Pacific Ocean. *Geophysical Research Letters*, *43*, 8645–8653. https://doi.org/10.1002/2016GL070226

Peña, M. A., Nemcek, N., & Robert, M. (2019). Phytoplankton responses to the 2014–2016 warming anomaly in the northeast subarctic Pacific Ocean. *Limnology & Oceanography*, *64*(2), 515–525. https://doi.org/10.1002/lno.11056

Plant, J. N., Johnson, K. S., Sakamoto, C. M., Jannasch, H. W., Coletti, L. J., Riser, S. C., & Swift, D. D. (2016). Net community production at Ocean Station Papa observed with nitrate and oxygen sensors on profiling float. *Global Biogeochemical Cycles*, *30*, 898–919. https://doi.org/10.1002/2015GB005349

Reynolds, R. W., Smith, T. M., Liu, C., Chelton, D. B., Casey, K. S., & Schlax, M. G. (2007). Daily high-resolution-blended analyses for sea surface temperature. *Journal of Climate*, *20*(22), 5473–5496. https://doi.org/10.1175/2007JCLI1824.1

Roesler, C., Uitz, J., Claustre, H., Boss, E., Xing, X., Organelli, E., et al. (2017). Recommendations for obtaining unbiased chlorophyll estimates from in situ chlorophyll fluorometers: A global analysis of WET Labs ECO sensors. *Limnology and Oceanography: Methods*, *15*(6), 572–585. https://doi.org/10.1002/lom3.10185

Saba, V. S., Friedrichs, M. A. M., Antoine, D., Armstrong, R. A., Asanuma, I., Behrenfeld, M. J., et al. (2011). An evaluation of ocean color model estimates of marine primary productivity in coastal and pelagic regions across the globe. *Biogeosciences*, *8*(2), 489–503. https://doi.org/10.5194/bg-8-489-2011

Saba, V. S., Friedrichs, M. A. M., Carr, M. E., Antoine, D., Armstrong, R. A., Asanuma, I., et al. (2010). Challenges of modeling depth-integrated marine primary productivity over multiple decades: A case study at BATS and HOT. *Global Biogeochemical Cycles*, *24*, GB3020. https://doi.org/10.1029/2009GB003655

Scannell, H. A., Johnson, G. C., Thompson, L., Lyman, J. M., & Riser, S. C. (2020). Subsurface evolution and persistence of marine heatwaves in the Northeast Pacific. *Geophysical Research Letters*, *47*, e2020GL090548. https://doi.org/10.1029/2020GL090548

Sheng, M. A., Xiaofeng, Y., Zui, T., Ziwei, L., & Xuan, Z. (2014). Assessment of uncertainties of ocean color parameters for the ocean Carbon-based Productivity Model. *IOP Conference Series: Earth and Environmental Science*, *17*(1), 012102. https://doi.org/10.1088/1755-1315/17/1/012102

Siegel, D. A., Buesseler, K. O., Behrenfeld, M. J., Benitez-Nelson, C. R., Boss, E., Brzezinski, M. A., et al. (2016). Prediction of the Export and Fate of Global Ocean Net Primary Production: The EXPORTS Science Plan. *Frontiers in Marine Science*, *3*, 1–10. https://doi.org/10.3389/fmars.2016.00022

Smale, D. A., Wernberg, T., Oliver, E. C. J., Thomsen, M., Harvey, B. P., Straub, S. C., et al. (2019). Marine heatwaves threaten global biodiversity and the provision of ecosystem services. *Nature Climate Change*, *9*, 306–312. https://doi.org/10.1038/s41558-019-0412-1

Theys, N., Hedelt, P., Smedt, I. D., Lerot, C., Yu, H., Vlietinck, J., et al. (2019). Global monitoring of volcanic SO_2 degassing with unprecedented resolution from TROPOMI onboard Sentinel-5 Precursor. *Scientific Reports*, *9*, 2643. https://doi.org/10.1038/s41598-019-39279-y

Timmerman, A. H., & Hamme, R. C. (2021). Consistent relationships among productivity rate methods in the NE Subarctic Pacific. *Global Biogeochemical Cycles*, *35*, e2020GB006721. https://doi.org/10.1029/2020GB006721

Trainer, V. L., Kudela, R. M., Hunter, M. V., Adams, N. G., & Mccabe, R. M. (2020). Climate extreme seeds a new domoic acid hotspot on the US West Coast. *Frontiers in Climate*, *2*, 1–11. https://doi.org/10.3389/fclim.2020.571836

Volk, T., & Hoffert, M. I. (1985). Ocean carbon pumps: Analysis of relative strengths and efficiences in ocean-driven atmospheric CO_2 changes. In E. Sundquist & W. Broecker (Eds.), *The carbon cycle and atmospheric CO2: Natural variations Archean to present*. AGU. https://doi.org/10.1029/GM032p0099

Welschmeyer, N. A., Strom, S., Goericke, R., DiTullio, G., Belvin, M., & Petersen, W. (1993). Primary production in the subarctic Pacific Ocean: Project SUPER. *Progress in Oceanography*, *32*(1–4), 101–135. https://doi.org/10.1016/0079-6611(93)90010-B

Westberry, T. K., Behrenfeld, M. J., Siegel, D. A., & Boss, E. (2008). Carbon-based primary productivity modeling with vertically resolved photoacclimation. *Global Biogeochemical Cycles*, *22*, GB2024. https://doi.org/10.1029/2007GB003078

Westberry, T. K., Schultz, P., Behrenfeld, M. J., Dunne, J. P., Hiscock, M. R., Maritorena, S., et al. (2016). Annual cycles of phytoplankton biomass in the subarctic Atlantic and Pacific Ocean. *Global Biogeochemical Cycles*, *30*, 175–190. https://doi.org/10.1002/2015GB005276

Westberry, T. K., Shi, Y. R., Yu, H., Behrenfeld, M. J., & Remer, L. A. (2019). Satellite-detected ocean ecosystem response to volcanic eruptions in the Subarctic Northeast Pacific Ocean. *Geophysical Research Letters*, *46*, 11270–11280. https://doi.org/10.1029/2019GL083977

Whitney, F. A., & Freeland, H. J. (1999). Variability in upper-ocean water properties in the NE Pacific Ocean. *Deep-Sea Research Part II: Topical Studies in Oceanography*, *46*(11–12), 2351–2370. https://doi.org/10.1016/S0967-0645(99)00067-3

Williams, N. L., Juranek, L. W., Johnson, K. S., Feely, R. A., Riser, S. C., Talley, L. D., et al. (2016). Empirical algorithms to estimate water column pH in the Southern Ocean. *Geophysical Research Letters*, *43*, 3415–3422. https://doi.org/10.1002/2016GL068539

Wong, C. S., Whitney, F. A., Crawford, D. W., Iseki, K., Matear, R. J., Johnson, W. K., et al. (1999). Seasonal and interannual variability in particle fluxes of carbon, nitrogen and silicon from time series of sediment traps at Ocean Station P, 1982–1993: Relationship to changes in subarctic primary productivity. *Deep-Sea Research Part II: Topical Studies in Oceanography*, *46*(11–12), 2735–2760. https://doi.org/10.1016/S0967-0645(99)00082-X

Wong, C. S., Whitney, F. A., Iseki, K., Page, J. S., & Zeng, J. (1995). Analysis of trends in primary productivity and chlorophyll-a over two decades at Ocean Station P (50°N, 145°W) in the Subarctic Northeast Pacific Ocean. In *Climate change and northern fish populations* (121st ed., pp. 107–117). Canadian Special Publication of Fisherires and Aquatic Sciences.

Xing, X., Claustre, H., Blain, S., D'Ortenzio, F., Antoine, D., Ras, J., & Guinet, C. (2012). Quenching correction for in vivo chlorophyll fluorescence acquired by autonomous platforms: A case study with instrumented elephant seals in the Kerguelen region (Southern Ocean). *Limnology and Oceanography: Methods*, *10*, 483–495. https://doi.org/10.4319/lom.2012.10.483

Xing, X., Claustre, H., Boss, E., Roesler, C., Organelli, E., Poteau, A., et al. (2017). Correction of profiles of in-situ chlorophyll fluorometry for the contribution of fluorescence originating from non-algal matter. *Limnology and Oceanography: Methods*, *15*(1), 80–93. https://doi.org/10.1002/lom3.10144

Yang, B., Emerson, S. R., & Angelica Penã, M. (2018). The effect of the 2013–2016 high temperature anomaly in the subarctic Northeast Pacific (the "blob") on net community production. *Biogeosciences*, *15*(21), 6747–6759. https://doi.org/10.5194/bg-15-6747-2018

Yang, B., Emerson, S. R., & Bushinsky, S. M. (2017). Annual net community production in the subtropical Pacific Ocean from in situ oxygen measurements on profiling floats. *Global Biogeochemical Cycles*, *31*, 728–744. https://doi.org/10.1002/2016GB005545

Yang, B., Fox, J., Behrenfeld, M. J., Boss, E. S., Haëntjens, N., Halsey, K. H., et al. (2021). In-situ estimates of net primary production in the Western North Atlantic with Argo profiling floats. *Journal of Geophysical Research: Biogeosciences*, *126*, e2020JG006116. https://doi.org/10.1029/2020JG006116

Yang, Q., Cokelet, E. D., Stabeno, P. J., Li, L., Hollowed, A. B., Palsson, W. A., et al. (2019). How "The Blob" affected groundfish distributions in the Gulf of Alaska. *Fisheries Oceanography*, *28*(4), 434–453. https://doi.org/10.1111/fog.12422